

## Assessment of Left Ventricular Viscoelastic Components Based on Ventricular Harmonic Behavior

ARASH KHERADVAR,<sup>\*,‡</sup> MICHELE MILANO,<sup>\*</sup> ROBERT C. GORMAN,<sup>†</sup> JOSEPH H. GORMAN, III,<sup>†</sup> and MORTEZA GHARIB<sup>\*</sup>

Published online: 17 June 2006

**Background:** Assessment of left ventricular (LV) function with an emphasis on contractility has been a challenge in cardiac mechanics during the recent decades. The LV function is usually described by the LV pressure-volume (P-V) relationship. Based on this relationship, the ratio of instantaneous pressure to instantaneous volume is an index for LV chamber stiffness. The standard P-V diagrams are easy to interpret but difficult to obtain and require invasive instrumentation for measuring the corresponding volume and pressure data. In the present study, we introduce a technique that can estimate viscoelastic properties, not only the elastic component but also the viscous properties of the LV based on oscillatory behavior of the ventricular chamber and it can be applied non-invasively as well. **Materials and Methods:** The estimation technique is based on modeling the actual long axis displacement of the mitral annulus plane toward the cardiac base as a linear damped oscillator with time-varying coefficients. Elastic deformations resulting from the changes in the ventricular mechanical properties of myocardium are represented as a time-varying spring while the viscous components of the model include a time-varying viscous damper, representing relaxation and the frictional energy loss. To measure the left ventricular axial displacement ten healthy sheep underwent left thoracotomy and sonomicrometry transducers were implanted at the apex and base of the LV. The time-varying parameters of the model were estimated by a standard Recursive Linear Least

Squares (RLLS) technique. **Results:** LV stiffness at end-systole and end-diastole was in the range of 61.86–136 dyne/g.cm and 1.25–21.02 dyne/g.cm, respectively. Univariate linear regression was performed to verify the agreement between the estimated parameters, and the measured values of stiffness. The averaged magnitude of the stiffness and damping coefficients during a complete cardiac cycle were estimated as  $58.63 \pm 12.8$  dyne/g.cm and 0 dyne.s/g.cm, respectively. **Conclusion:** The results for the estimated elastic coefficients are consistent with the ones obtained from force-displacement diagram. The trend of change in the estimated parameters is also in harmony with the previous studies done using P-V diagram. The only input used in this model is the long axis displacement of the annulus plane, which can also be obtained non-invasively using tissue Doppler or MR imaging.

**Key words:** left ventricle; diastole; systole; cardiac modeling; contractility; viscoelasticity.

### INTRODUCTION

Assessment of left ventricular function with an emphasis on contractility has been a major challenge in cardiac mechanics during the recent decades. To date, extensive work has been done to develop models describing left ventricular (LV) dynamics. An excellent series of publications by Suga and Sagawa (1974), Yellin *et al.* (1990, 1986), Weiss (1976), Peskin (2000) and other researchers ultimately resulted in a more precise conceptual understanding of how the heart works. However, an applicable model that can differentiate between different pathophysiological states based on mechanical properties of the heart is still needed.

In regards to describing ventricular function, Suga and Sagawa introduced a diagram for instantaneous

<sup>\*</sup>Cardiovascular and Biofluid Dynamics Laboratory, California Institute of Technology, Pasadena, CA.

<sup>†</sup>Harrison Department of Surgical Research, University of Pennsylvania School of Medicine, Philadelphia, PA.

<sup>‡</sup>To whom correspondence should be addressed at Cardiovascular and Biofluid Dynamics Laboratory, California Institute of Technology, 301-46, Caltech, 1200 E California Blvd., Pasadena, CA 91125; e-mail: arashkh@caltech.edu

ventricular pressure-volume (P-V) relationship. Based on their diagram (Suga and Sagawa, 1974), they described the ratio of instantaneous pressure to instantaneous volume ( $P(t)/(V(t) - V_d)$ ) as the time varying stiffness of ventricular chamber. The standard P-V diagrams are easy to interpret and give a rough estimate of the mechanical work done by the LV (Takaoka *et al.*, 1992). However, the pressure and the corresponding volume of the LV need to be measured invasively using sophisticated techniques, such as intravascular micromanometers and conductance catheters (Applegate *et al.*, 1990), which restrict the clinical applications of this model. Furthermore, this model ignores the viscoelasticity of the heart by not considering viscous damping. It has also been shown that although  $dp/dv$  provides a useful description of simultaneous LV pressure and volume events, it does not represent actual LV physical properties (Burkhoff *et al.*, 1993; Campbell *et al.*, 1990, 1991; Shroff *et al.*, 1993).

Templeton and Nardizzi (1974) implemented a different model based on perturbations of left ventricular pressure and volume. They described a second order linear differential equation for pressure with ventricular volume displacement as the model input. The model was then used to describe nominal elastic and viscous coefficients for the ventricle. However, their time varying coefficients were computed from an externally applied sinusoidal volume change rather than the naturally existing absolute volume and pressure of the ventricle. Additionally, this model was also dependant on obtaining LV pressure data in response to some LV volume perturbations, which makes the model almost impossible to use for clinical applications.

Recently Campbell *et al.* (2005) proposed a novel mathematical model that relates LV pressure-volume relationships to cardiac myocyte force-length dynamics in rat's hearts. This sophisticated model makes the beating heart amenable to studies that aim the relevance of myofilament contractile behavior to cardiac system function. However, the parameters inferred from this model mostly reflect the contractile parameters at cellular level rather than global state of the heart.

A more applicable model for diastolic function that uses Doppler velocity profile input has been developed by Kovacs *et al.* (1987). Their motivation was the similarity between the LV during diastole as a suction pump and a damped harmonic oscillator. They used a linear differential equation that describes the motion of a forced, damped harmonic oscillator with constant coefficients. The forcing term of the model was set to zero during early diastole and to a sinusoidal forcing term during atrial contraction. Kovacs' *et al.* used an approximation of the

transmitral jet velocity obtained from Doppler echocardiography to validate their model. Despite the fact that their model only describes diastolic function, the major advantage of the Kovacs' model to other existing ones is its simplicity. However, recent technological advances in ultrasound techniques allow for accurate, direct measurements of annulus displacement, thus paving the way for the use of more sophisticated modeling techniques, capable of describing the entire cardiac cycle.

In the present study, we use a technique to assess the LV contractile behavior during the entire cardiac cycle. The estimation technique is based on modeling the actual long axis displacement of the mitral annulus plane toward the cardiac base as a linear damped oscillator with time-varying coefficients. We derive longitudinal rather than global indexes of stiffness and damping of the left ventricle. Elastic deformations resulting from the changes in the ventricular mechanical properties of myocardium are represented as a time-varying spring. The viscous components of the model include a time-varying viscous damper, representing relaxation and the frictional energy loss. Thus, one would expect the ventricular viscous properties to reflect the force-velocity behavior of cardiac muscle translated into ventricular level (Hunter *et al.*, 1983). The nominal oscillator also has structural similarities to internal viscoelastic loading in papillary muscles (Chiu *et al.*, 1982a, 1982b) and myocytes resembling Voigt's model of viscoelasticity (Schmiel *et al.*, 2005).

## METHOD

### Mathematical Model

Longitudinal displacement of the mitral annulus plane toward the apex during a cardiac cycle was considered analogous to the motion of a damped harmonic oscillator with time-varying coefficients. The time dependency of the coefficients is an advantage of this model to the existing ones (Kovacs *et al.*, 1987; Rich *et al.*, 1999) and allows the model to describe systole, diastole and the transitional isovolumic phases of the cardiac cycle. This is consistent with the fact that the LV acts as two distinct pumps in a cardiac cycle; acting as a suction pump (Brecher, 1956; Firstenberg *et al.*, 2001; Ling *et al.*, 1979; Nikolic *et al.*, 1995) during diastole and as a positive displacement pump during systole in which the pressure in the chamber depends on the walls displacement and the blood volume (Burkhoff and Sagawa, 1986; Burkhoff *et al.*, 2005).

Due to the natural time-dependency of the LV mass (blood and tissue), identification of LV mass, separated from the rest of the heart, as a function of time was impractical. Therefore, the equation of motion for a linear harmonic oscillator with time varying coefficients was divided by the instantaneous mass of the system and rewritten as:

$$\ddot{y} + h(t)\dot{y} + K(t)y = 0 \quad (1)$$

where  $(y)$  is the zero-mean displacement of the system and  $(x)$  is the longitudinal base to apex displacement (table 1):

$$y = (x - \bar{x}) \quad (2)$$

The bar indicates mean value, the dot denotes differentiation with respect to time and “ $h$ ” and “ $K$ ” are the damping and elastic (stiffness) coefficients per unit mass, respectively. Equation (1) can also be reorganized to a constant-coefficient harmonic oscillator with time varying forcing term, as follows:

$$\ddot{y} + \bar{h}\dot{y} + \bar{K}y = (\bar{h} - h(t))\dot{y} + (\bar{K} - K(t))y \quad (3)$$

In (3), “ $\bar{h}$ ” and “ $\bar{K}$ ” are the averaged values of damping ( $h$ ) and stiffness ( $K$ ) coefficients during a cardiac cycle, respectively. The function on the right-hand side of (3) is the intrinsic forcing function, which can be a representative of contractile elements of the left ventricle (Cazorla *et al.*, 2001; Fukuda *et al.*, 2001; Granzier and Labeit, 2004). The intrinsic forcing function is described as:

$$f(t) = (\bar{h} - h(t))\dot{y} + (\bar{K} - K(t))y \quad (4)$$

**Table 1. Abbreviations and acronyms**

$x$	longitudinal base to apex displacement
$y$	zero-mean displacement
$\bar{K}$	mean of stiffness coefficient
$K_{ED}$	end diastolic stiffness coefficient
$K_{ES}$	end systolic stiffness coefficient
$\bar{h}$	mean of damping coefficient
$f_p$	Force density
$\mu_K$	mean of the mean of stiffness coefficient
$\mu_h$	mean of the mean of damping coefficient
$i$	sample index
$\mathbf{P}_i$	covariance matrix of the estimated parameters
$\lambda$	smoothing (forgetting) factor
$e_i$	estimation error
$\mathbf{G}_i$	adaptive estimator gain
$\mathbf{I}$	identity matrix
$t$	time

Considering that we measure the longitudinal displacement “ $x(t)$ ”, the parameters in this model, as well as the forcing function, can be estimated by using a standard identification technique (Ljung, 1987), which will be described in details after the description of the data acquisition procedure.

## Animal Preparation

In order to assess the model behavior, an animal study with limited cases was performed with Dorset sheep. Animal data was collected at the Harrison department of surgical research, University of Pennsylvania School of Medicine. Animals were treated under an experimental protocol approved by the University of Pennsylvania’s Institutional Animal Care and Use Committee (IACUC) and in compliance with NIH publication No. 85-23 as revised in 1985. Animals were induced with Thiopental sodium (10–15 mg/kg intravenously [IV]) and intubated. Anesthesia was maintained with Isoflurane (1.5–2%) and oxygen. All animals received Glycopyrrolate (0.4 mg IV) and Enrofloxin (10 mg/kg IV) on induction. To measure the left ventricular axial displacement and intraventricular pressure, 10 healthy sheep between 35 and 45 kg underwent left thoracotomy after induction of anesthesia. Sonomicrometry transducers (1.0 mm; Sonometrics Corp., London, Ontario, Canada) were implanted at the apex and the base of the LV to measure their mutual distance. The surface electrocardiogram (ECG), arterial blood pressure (ABP) and left ventricular pressure (LVP) were continuously monitored and recorded. LVP was measured using a high-fidelity pressure transducer (Spc-350, Millar Instruments Inc., Houston, TX) inserted from the femoral artery into the left ventricle. Different phases of the cardiac cycle were defined based on the trend of  $dP/dt$  in each case and the results confirmed by the ECG.

## Equation of Motion and Parameter Estimation

The relative displacements obtained from sonomicrometry transducers were substituted in Eq. (1). The problem of tracking the parameters was tackled by resorting to a class of recursive linear least squares algorithms (Ljung, 1987). To estimate the model parameters (table 1), Eq. (1) was re-written as:

$$y = -h\dot{y} - Ky = \boldsymbol{\theta} \cdot \boldsymbol{\varphi}^T \quad (5)$$

where  $\boldsymbol{\theta} = \{h, K\}^T$ , and  $\boldsymbol{\varphi} = \{-\dot{y}, -y\}^T$ . The coefficients  $\boldsymbol{\theta}$  are estimated by a standard Recursive Linear Least Squares (RLLS) technique. Putting a ‘hat’ symbol on top of the estimated quantities, the RLLS equations read:

$$\mathbf{P}_{i+1} = \frac{1}{\lambda} (\mathbf{I} - \mathbf{G}_i \hat{\boldsymbol{\varphi}}_i^T) \mathbf{P}_i \quad (6)$$

where  $i$  denotes the sample index;  $\mathbf{I}$  is the  $2 \times 2$  identity matrix;  $\mathbf{P}_i$  is the covariance matrix of the estimated parameters;  $\mathbf{G}_i$  is the adaptive estimator gain; and the scalar  $\lambda$  adjusts the smoothing of the estimations (i.e. the closer  $\lambda$  to one, the smoother the estimation: typical values for this parameter are between 0.9 and 0.99). The adaptive estimator tracks the time varying coefficients, and then an estimation of the forcing term is obtained by computing the averaged coefficients and using Eq. (3). The model parameters (table 1) are updated by computing the estimation error ( $e_i$ ) for the second derivative, as follows:

$$e_i = \hat{y}_i - \boldsymbol{\theta}_i \cdot \hat{\boldsymbol{\varphi}}_i^T \quad (7)$$

The estimation error is used to update the estimate for the model parameters:

$$\boldsymbol{\theta}_{i+1} = \boldsymbol{\theta}_i + \mathbf{G}_i e_i \quad (8)$$

where  $\mathbf{G}_i$  is the linear estimator gain (table 1). The optimal value for the estimator gain  $\mathbf{G}_{i+1}$  for use in the next step is computed as a function of the covariance matrix  $\mathbf{P}_{i+1}$ :

$$\mathbf{G}_{i+1} = \frac{\mathbf{P}_{i+1} \hat{\boldsymbol{\varphi}}_i}{\lambda + \hat{\boldsymbol{\varphi}}_i^T \mathbf{P}_{i+1} \hat{\boldsymbol{\varphi}}_i} \quad (9)$$

The RLLS technique improves the parameter estimation by sequentially processing each sample. In order to make the estimator maximally responsive in the initial adaptation phase, the starting value for the covariance matrix  $\mathbf{P}_0$  is set at  $1000 \times \mathbf{I}$ . The starting value for the parameters is chosen to be zero. Each step of the RLLS algorithm updates the covariance matrix of the predictions  $\mathbf{P}_{i+1}$  by using current measurements, as in Eq. (6). The RLLS also improves the parameters estimation by predicting a measured quantity with (5), using current values of the parameters. Equation (7) computes the estimation error, which is used in Eq. (8) to improve the estimated parameter by means of an adaptive correction gain computed in Eq. (9).

Equation (1) is chosen as a continuous time model to make the physical interpretation of the parameters easier.

However, in Eqs. (6) through (9), discrete samples of the first and second derivatives of the measured displacement were used. Due to the presence of noise in the measured data and the effects of sampling rate, care was taken, while approximating these quantities with finite differences, to prevent the quantities from diverging. Söderström *et al.* (1997) thoroughly described the crucial choice of a suitable estimator for the derivatives. In the present study, we use an estimator for the derivatives compatible with the RLLS technique (Ljung, 1987).

## RESULTS

Based on our model, the system can be studied as an unforced damped harmonic oscillator with time-varying coefficients (1), or a forced damped harmonic oscillator with constant coefficients (3).

### Unforced Model with Time-Varying Coefficients

Temporal evolutions in stiffness (elasticity) and damping of the system within a cardiac cycle is extracted from the unforced form of the oscillator (1). Stiffness and damping coefficients of the system for each individual case are estimated as a function of time, based on the RLLS algorithm (Eqs. (6) through (9)). Time evolution of the stiffness and damping coefficients used in the unforced form of the model are shown in Figs. 1 and 2.

Since the estimated coefficients for “ $K$ ” were obtained from a one-dimensional model of the LV, their magnitudes represent longitudinal stiffness rather than the actual stiffness of the ventricle. Therefore, the magnitude of stiffness at the end-systole and the end-diastole do not have the same dimension as the results of the previous studies based on P-V curve (Suga and Sagawa, 1974; Kass and Maughan, 1988; Chen *et al.*, 2001). However, to verify the accuracy of the results estimated by the model, we described a nominal force-displacement ( $f_{p-x}$ ) diagram equivalent to Suga and Sagawa’s (1974) P-V diagram. In this diagram, instead of LV volume, long axis displacement is used, and the pressure is replaced by the force density per unit mass ( $f_p$ ), defined as LV pressure times unit area divided by the heart mass. The measured  $f_p$  for each case is plotted against the longitudinal displacement of the mitral annulus (Fig. 3). Based on our definitions, the slopes of this curve at the end-systole and the end-diastole have a dimension equivalent to the estimated “ $K$ .” The results for the oscillator’s stiffness coefficient and  $f_{p-x}$

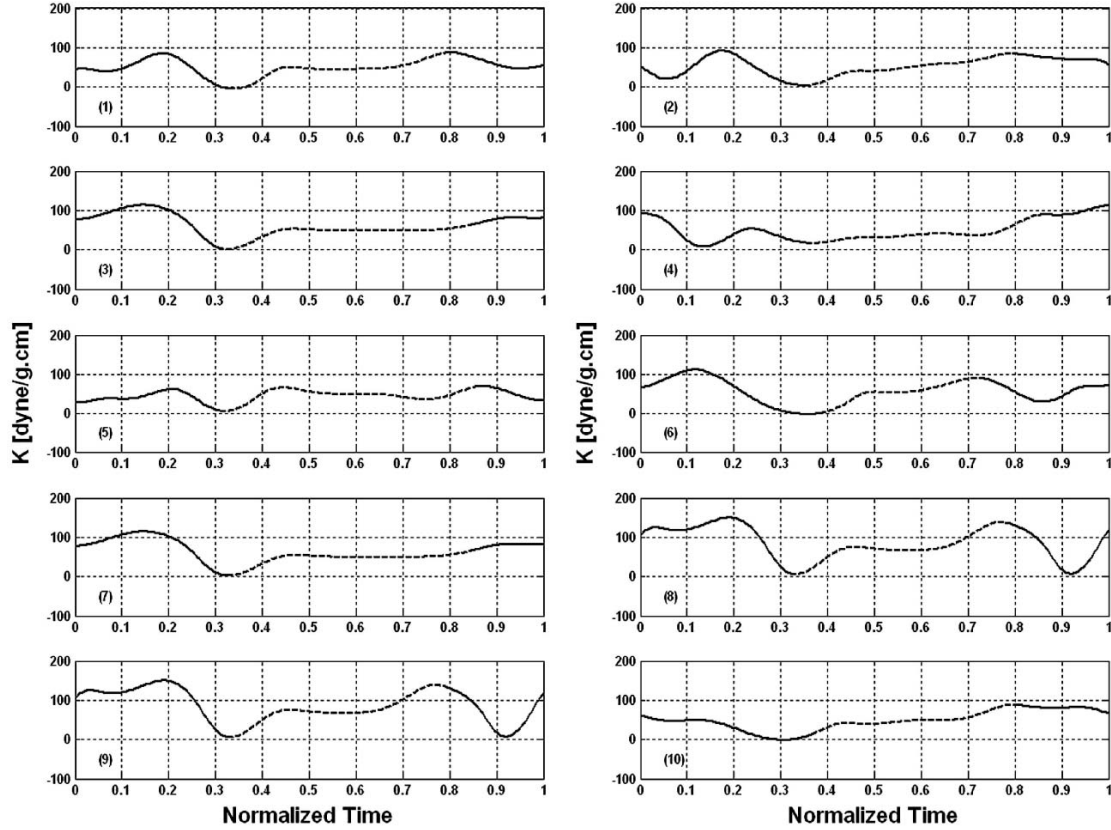


Figure 1. Time evolution of stiffness coefficients for all the 10 cases. Dotted lines indicates systole; continuous line indicates diastole.

diagram stiffness at the end-systole and the end-diastole are provided in Table 2.

Univariate linear regression was performed to test the agreement between the model's estimation, and the measured values of "K" from  $f_{p-x}$  diagram. Bland-Altman analysis (Bland and Altman, 1986) was also employed to evaluate systematic bias in the correlation. Statistical analysis was performed using *STATA* statistical software (version SE 8.00, STATA corporation college Station, Texas).

Figure 4 displays group regression and Bland-Altman plots for 10 comparisons between model-estimated stiffness and pressure-Displacement measured "K" at end-systole and end-diastole, respectively. The regression equation for  $K_{ES}$  is  $K_{ES} = 0.5357 K_{ESf_{p-x}} + 42.3460$  ( $R^2 = 0.7141$ ,  $p < 0.002$ ). Correlation coefficient between two data sets is 0.8450. The mean difference is 0.543 dyne/g.cm ( $p = 0.910$ , 95% confidence interval:  $-10.03$ , 11.12) that means no systematic bias. For  $K_{ED}$ , the regression equation is  $K_{ED} = 0.7046 K_{ESf_{p-x}} + 2.8758$  ( $R^2 = 0.8253$ ,  $p < 0.00001$ ). The correlation coefficient between two data sets is 0.9084. The mean differ-

ence is  $0.675 K_{ESf_{p-x}}$  dyne/g.cm ( $p = 0.465$ , 95% confidence interval:  $-1.32$ , 2.67) and therefore, no systematic bias exists.

### Forced Model with Constant Coefficients

The forced form of the oscillator (3) provides information about the global (averaged) state of elasticity and damping of the system, in addition to the instantaneous intrinsic longitudinal force generated over a cardiac cycle.

Values of mean stiffness and damping coefficients for each case used in the forced form of the Eq. (3) are provided in Table 2. To determine whether the coefficients were from the same distribution and possessed the same mean, we applied Student's *t*-test for each sample of coefficients. For each coefficient of stiffness and damping, we calculated the mean of the means of all 10 cases,  $\mu_k$  and  $\mu_h$ , respectively. Then the null hypothesis that each sample of coefficients had the same mean as " $\mu_k$ " and " $\mu_h$ " was tested. The estimated " $\mu_k$ " and " $\mu_h$ " for 10 healthy cases were  $58.63 \pm 12.8$  dyne/g.cm and zero dyne.s/g.cm,

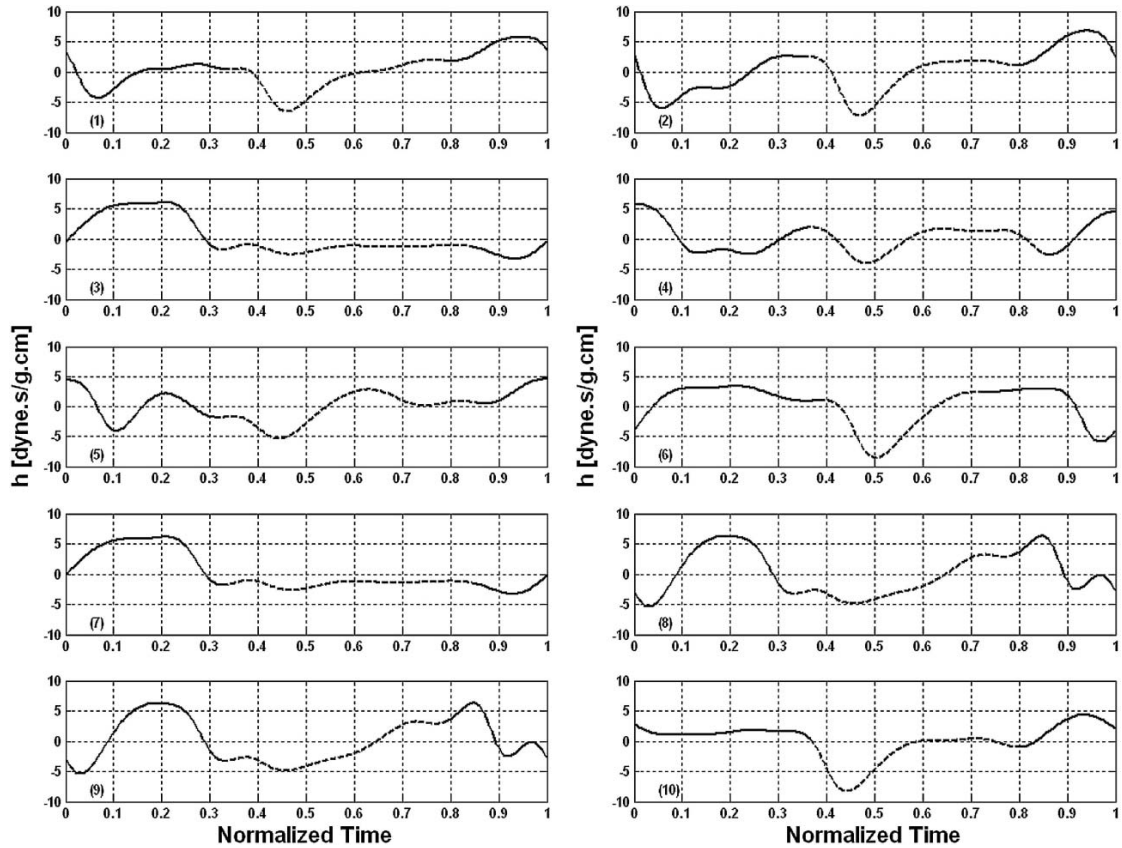


Figure 2. Time evolution of damping coefficients for all the 10 cases. Dotted lines indicates systole; continuous line indicates diastole.

respectively. The  $p$ -value for each sample is shown in Table 2.

The forcing term of Eq. (3) was also computed based on (4), using the estimated parameters, zero-mean longitudinal displacement ( $y$ ) and zero-mean longitudinal velocity ( $\dot{y}$ ). Evolution of the forcing term within a cardiac cycle is shown in Fig. 5. Incident of diastole and systole were determined based on simultaneous ECG and the LV pressure measurements.

## DISCUSSION

We developed a technique that employs a dynamic model for longitudinal displacement of the annulus plane toward the apex. Using this technique enables us to estimate longitudinal elastic and damping coefficients for the left ventricle based only on the mitral annulus displacement. Although the estimated values of coefficients were considered as one-dimensional parameters, their time-

varying trends were consistent with the previous studies that considered  $dP/dV$  as an index of stiffness (Suga and Sagawa, 1974; Chen *et al.*, 2001) and gave quantitative information about LV dynamics. The only input used in this model is the long axis displacement of the annulus plane, which can also be obtained non-invasively using tissue Doppler. The fact that the technique can be used as a non-invasive way to evaluate LV function is the key advantage of this model with respect to existing techniques.

As it can be observed from Fig. 2, in all the cases, the stiffness of the model has a minimum at the end-diastole, increases during systole and reaches a maximal peak at the end-systole. This observation is consistent with the  $f_{p-x}$  diagram plotted based on measured data (Fig. 3), with the P-V diagram of Suga and Sagawa (Suga and Sagawa, 1974) and with the other models that describe LV stiffness based on P-V relationship (Campbell *et al.*, 1990, 1991; Hunter *et al.*, 1983; Firstenberg *et al.*, 2001; Chen *et al.*, 2001).

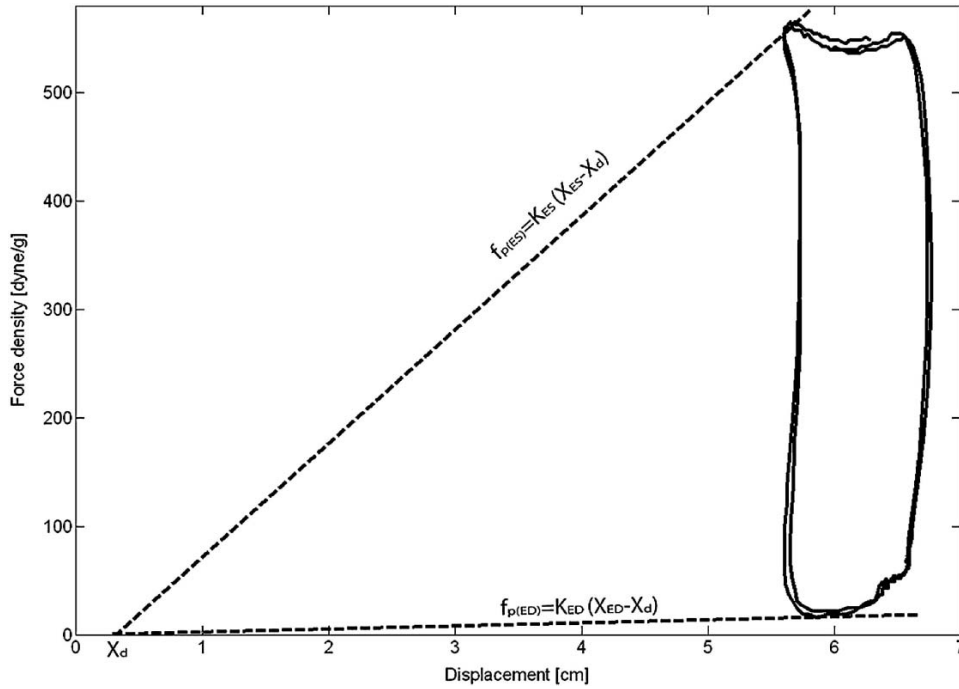


**Figure 3.** Plot of the force density of a representative case against the longitudinal displacement of the mitral annulus. See text for the definition of the force density ( $f_p$ ).  $x_d$  is the displacement axis intercept of the tangent lines.

Estimation of damping coefficient gives additional information on ventricular contractile behavior with respect to the estimated elastic component data. The estimated damping coefficient for the system had a zero mean value, and its range of variation was between  $-10$  and  $10$  dyne.s/g.cm (Fig. 5). The coefficient showed a negative peak during systole. Considering the fact that the stiffness coefficient is always positive and greater than

the damping coefficient during systole (Figs. 1 and 2), it can be inferred from the linearized stability analysis (Haberman, 1998) that the equilibrium solution is unstable for each time point in which “ $h$ ” is less than zero. This means that the displacement of the system grows (usually exponentially). This can be a justification for the sharp longitudinal displacement of the mitral annulus plane toward the apex during systole.

**Table 2. Magnitude of Coefficients**

	$\bar{K}$ (dyne/g.cm)		$\bar{h}$ (dyne.s/g.cm)		$K_{ES}$ (dyne/g.cm)		$K_{ED}$ (dyne/g.cm)	
	Magnitude	<i>P</i> -value	Magnitude	<i>P</i> -value	Measured	Estimated	Measured	Estimated
Sheep 1	49.11	0.16	0.05	0.90	74.5	85.81	2.15	2
Sheep 2	51.32	0.50	0.02	0.90	98.33	83.83	8.73	5.84
Sheep 3	62.39	0.39	0.09	0.68	70.35	61.86	3.12	1.25
Sheep 4	47.16	0.12	0.01	0.64	96.67	89.64	12.2	16.62
Sheep 5	44.40	0.05	0.04	0.79	74.17	68.74	5.69	4.8
Sheep 6	56.86	0.83	0.04	0.79	100	86.41	4.33	5.43
Sheep 7	63.62	0.15	0.07	0.70	71.52	66.86	5.2	3.42
Sheep 8	83.40	0.05	0.12	0.68	111.25	134.5	11.22	7.07
Sheep 9	83.48	0.05	0.12	0.68	111.25	136	10.59	7.07
Sheep 10	47.84	0.06	0.02	0.85	97.83	86.79	18.04	21.02

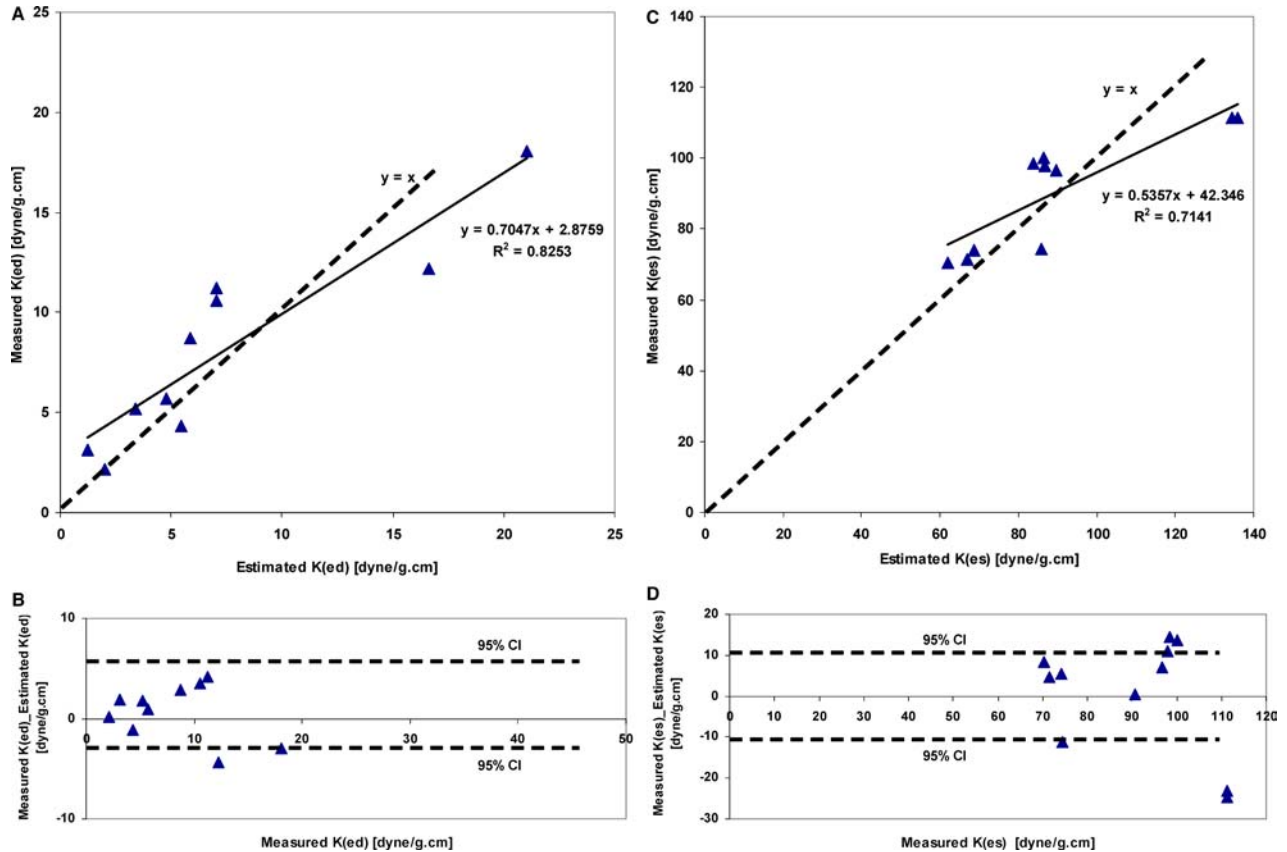


**Figure 4.** (A) Linear regression (solid line) and the line of identity (dotted line) comparing estimated left ventricular stiffness ( $K_{ED}$ ) at end-diastole derived by harmonic oscillator model and by force-displacement diagram for 10 sheep. (B) Bland-Altman plot of difference between measured and estimated ( $K_{ED}$ ) versus mean value. Mean and 95% confidence interval of the mean difference are shown. (C) Linear regression (solid line) and the line of identity (dotted line) comparing estimated left ventricular stiffness ( $K_{ES}$ ) at end-diastole derived by harmonic oscillator model and by force-displacement diagram for 10 sheep. (D) Bland-Altman plot of difference between measured ( $K_{ES}$ ) and estimated ( $K_{ES}$ ) versus mean value. Mean and 95% confidence interval of the mean difference are shown.

Although there are quite a number of published articles about the stiffness of LV chamber, less attention has been paid to viscous damping in the left ventricle. However, measured global damping of left ventricle over a cycle can also be used as an index for evaluation of cardiac functionality. There are recent papers that have studied the damping characteristics of myocardial contractile elements at cellular level (Opitz *et al.*, 2003; Kulke *et al.*, 2001). Nevertheless, to our best knowledge, there have been no published articles relating viscous damping at the cellular level to the global damping of the left ventricle as a continuum.

Time-varying behavior of stiffness and damping coefficients can be incorporated into an intrinsic forcing term (4) of an equivalent harmonic oscillator with constant coefficients (3). This forcing term shows periodic behavior

over cardiac cycles and has a maximal positive peak at the end-diastole. However, other than the maximal peak at the end-diastole, no other features can be observed in common in all the cases (Fig. 5). This may imply that the intrinsic forces generated by cardiac contractile elements are naturally complex and are not showing the same patterns in different hearts. Literature reports (Cazorla *et al.*, 2001; Fukuda *et al.*, 2001; Granzier and Labeit, 2004; Opitz *et al.*, 2003) suggest that myocardial contractile elements (e.g. titin) may affect active force generation in the heart. The present model confirms the existence of such an intrinsic active force in the left ventricle without articulating about its origin.

Another interesting observation resulting from the forced form of the oscillator is the similarity between the magnitude of  $\bar{K}$  and  $\bar{h}$  in all the 10 cases ( $p > 0.05$ ). Based

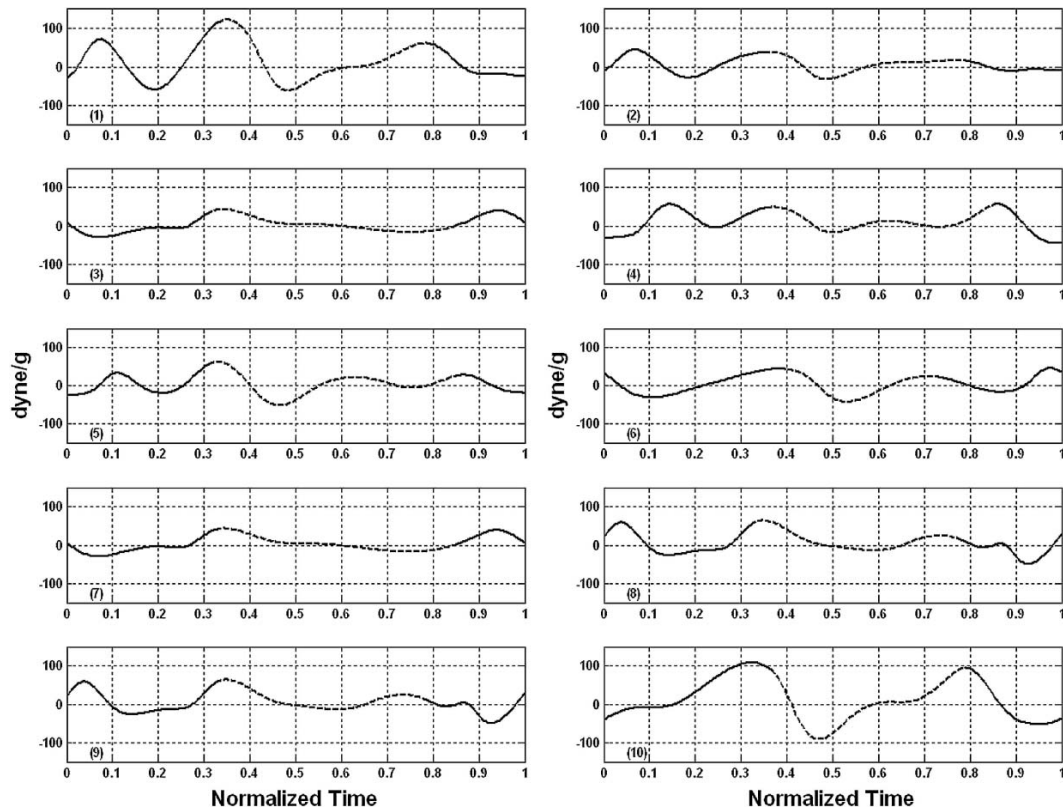


Figure 5. Time evolution of forcing term for all the 10 cases. Dotted lines indicates systole; continuous line indicates diastole

on the present model, the mean damping coefficient can be considered zero in healthy hearts, denoting that the viscous damping is minimal in normal LV. Further studies are in progress to observe the variation of coefficients in cases where the physical state of the LV has been changed due to acquired or congenital heart diseases.

## ACKNOWLEDGMENTS

This work is partially supported by NIH grants HL-63954, HL-71137, HL-73021 and HL-76560.

## REFERENCES

- Applegate RJ, Cheng CP, and Little WC. Simultaneous conductance catheter and dimension assessment of left ventricular volume in the intact animal. *Circulation* 81: 638–648, 1990.
- Bland JM, and Altman DG. Statistical methods for assessing agreement between two methods of clinical measurement. *Lancet* xx: 307–310, 1986.
- Brecher GA. Experimental evidence of ventricular diastolic suction. *Circ Res* 4: 513–518, 1956.
- Burkhoff D, de Tombe PP, and Hunter WC. Impact of ejection on the magnitude and time course of ventricular pressure generating capacity. *Am J Physiol Heart Circ Physiol* 265: H899–H909, 1993.
- Burkhoff D, Mirsky I, and Suga H. Assessment of systolic and diastolic ventricular properties via pressure-volume analysis: A guide for clinical, translational, and basic researchers. *Am J Physiol Heart Circ Physiol* 289: 501–512, 2005.
- Burkhoff D, and Sagawa K. Ventricular efficiency predicted by an analytical model. *Am J Physiol Regul Integr Comp Physiol* 250: R1021–R1027, 1986.
- Campbell KB, Kirkpatrick RD, Knowlton GG, and Ringo JA. Late systolic mechanical properties of the left ventricle: Deviation from elastance-resistance behavior. *Circ Res* 66: 218–233, 1990.
- Campbell KB, Shroff SG, and Kirkpatrick RD. Short time-scale LV systolic dynamics: Evidence for a common mechanism in both LV chamber and heart-muscle mechanics. *Circ Res* 68: 1532–1548, 1991.
- Campbell KB, Wu Y, Simpson AM, Kirkpatrick RD, Shroff SG, Granzier HL, and Slinker BK. Dynamic myocardial contractile parameters from left ventricular pressure volume measurements. *Am J Physiol Heart Circ Physiol*. 289: H114–H130, 2005.
- Cazorla O, Wu Y, Irving TC, and Granzier H. Titin-based modulation of calcium sensitivity of active tension in mouse skinned cardiac myocytes. *Circ Res* 88: 1028–1035, 2001.
- Chiu YL, Ballou EW, and Ford LE. Internal viscoelastic loading in cat papillary muscle. *Biophys J* 40: 109–120, 1982a.

- Chiu YL, Ballou EW, and Ford LE. Velocity transients and viscoelastic resistance to active shortening in cat papillary muscle. *Biophys J* 40: 121–128, 1982b.
- Chen CH, Fetcs B, Nevo E, Rochitte CE, Chiou KR, *et al.* Noninvasive Single-Beat Determination of Left Ventricular End-Systolic Elastance in Humans. *J Am Coll Cardiol* 38: 2028–2034, 2001.
- Firstenberg MS, Smedira NG, Greenberg NL, Prior DL, *et al.* Relationship between early diastolic intraventricular pressure gradients, an index of elastic recoil, and improvements in systolic and diastolic function. *Circulation* 104(12 Suppl 1): I330–I335, 18 Sep 2001.
- Fukuda N, Sasaki D, Ishiwata S, and Kurihara S. Length dependence of tension generation in rat skinned cardiac muscle: Role of titin in the Frank-Starling mechanism of the heart. *Circulation* 104: 1639–1645, 2001.
- Granzier HL, and Labeit S. The Giant Protein Titin: A Major Player in Myocardial Mechanics, Signaling, and Disease. *Circ Res* 94: 284–295, 2004.
- Haberman R. Mathematical models: Mechanical vibrations, population dynamics and traffic flow. *SIAM*, 1998.
- Hunter WC, Janicki JS, Weber KT, and Noordergraaf A. Systolic mechanical properties of the left ventricle. Effects of volume and contractile state. *Circ Res* 52: 319–327, 1983.
- Kass DA, and Maughan WL. From “Emax” to pressure-volume relations: A broader view. *Circulation* 77: 1203–1212, 1988.
- Kovacs SJ, Barzilai B, and Perez JE. Evaluation of diastolic function with Doppler echocardiography: The PDF formalism. *Am J Physiol Heart Circ Physiol* 252(1): H178–H187, Part 2, 1987.
- Kulke M, Fujita-Becker S, Rostkova E, Neagoe C, Labeit D, Manstein DJ, Gautel M, and Linke WA. Interaction between PEVK-titin and actin filaments: Origin of a viscous force component in cardiac myofibrils. *Ore Res* 89: 874–881, 2001.
- Ling D, Rankin JS, Edwards CH II, *et al.* Regional diastolic mechanics of the left ventricle in the conscious dog. *Am J Physiol* 236: H323–H330, 1979.
- Ljung L. System identification—Theory for the user, Prentice-Hall, Englewood Cliffs, NJ, 1987.
- McQueen DM, and Peskin CS. A three-dimensional computer model of the human heart for studying cardiac fluid dynamics. *Computer Graphics-US* 34(1): 56–60, Feb 2000.
- Nikolic SD, Feneley MP, Pajaro OE, *et al.* Origin of regional pressure gradients in the left ventricle during early diastole. *Am J Physiol* 268: H550–H557, 1995.
- Opitz CA, Kulke M, Leake MC, Neagoe C, Hinssen H, Hajjar RJ, and Linke WA. Damped elastic recoil of the titin spring in myofibrils of human myocardium. *Proc Natl Acad Sci USA* 100: 12688–12693, 2003.
- Rich MW, Stitzel NO, and Kovacs SJ. Prognostic value of diastolic filling parameters derived using a novel image processing technique in patients  $\geq 70$  years of age with congestive heart failure. *Am J Cardiol* 84(1): 82–86, 1999.
- Schmiel FK, Lorenzen N, Fischer G, Harding P, and Kramer HH. Diastolic left ventricular function Experimental study of the early filling period using the Voigt model. *Basic Res Cardiol* 100(1): 64–74, Jan 2005.
- Shroff SG, Campbell KB, and Kirkpatrick RD. Short time-scale LV systolic dynamics: Pressure vs. flow clamps and effects of activation. *Am J Physiol Heart Circ Physiol* 264: H946–H959, 1993.
- Söderström T, Fan H, Carlsson B, and Bigi S. Least Squares Parameter Estimation of Continuous-Time ARX models from Discrete-Time Data. *IEEE Trans. On Automatic Control* 42(5): 659–673, 1997.
- Suga H, and Sagawa K. Instantaneous pressure-volume relationships and their ratio in the excised, supported canine left ventricle. *Ore Res* 35: 117–126, 1974.
- Takaoka H, Takeuchi M, Odake M, and Yokoyama M. Assessment of myocardial oxygen consumption ( $V \sim O_2$ ) and systolic pressure-volume area (PVA) in human hearts. *Eur Heart J* 13: 85–90, 1992.
- Templeton GH, and Nardizzi LR. Elastic and viscous stiffness of the canine left ventricle. *J Appl Physiol* 36(1): 123–127, 1974.
- Weiss JL, Frederiksen JW, and Weisfeldt ML. Hemodynamic determinants of time-course of fall in canine left-ventricular pressure. *J Clin Invest* 58(3): 751–760 1976.
- Yellin EL, Hori M, Yoran C, Sonnenblick EH, *et al.* Left-ventricular relaxation in the filling and nonfilling intact canine heart. *Am J Cardiol: Part 2* 250(4): H620–H629, 1986.
- Yellin EL, Nikolic S, and Prater RWM. Left-ventricular filling dynamics and diastolic function. *Progress in Cardiovascular Diseases* 32(4): 247–271, 1990.